Nano Res. 2011, 4(8): 788–794
DOI 10.1007/s12274-011-0135-8
Research Article

ISSN 1998-0124
CN 11-5974/O4

Polarized Light Microscopy and Spectroscopy of Individual Single-Walled Carbon Nanotubes

Jacques Lefebvre (✉) and Paul Finnie (✉)

Institute for Microstructural Sciences, National Research Council, Ottawa, Canada K1A 0R6

Received: 23 February 2011 / Revised: 5 April 2011 / Accepted: 6 April 2011

ABSTRACT

Polarized light microscopy (PLM) is used to image individual single-walled carbon nanotubes (SWNTs) suspended in air across a slit opening. The imaging contrast relies on the strong optical anisotropy typical of SWNTs. We combine PLM with a tunable light source to enable hyperspectral excitation spectroscopy and nanotube chirality assignment. Comparison with fluorescence microscopy and spectroscopy confirms the assignment made with PLM. This represents a versatile new approach to imaging SWNTs and related structures.

KEYWORDS

Carbon nanotube, microscopy, luminescence, absorption, polarization, homodyne

1. Introduction

Carbon nanotubes are excellent candidates for optical microscopy. While the 1 nm scale cross-section of single-walled carbon nanotubes (SWNTs) is essentially molecular, the multi-micron to millimetre scale lengths of present day SWNTs are macroscopic and easily accessible to optics in the far field. In addition to the geometry, the optical signal from SWNTs is very strong, due to sharply peaked optical transition energies which occur mainly because of the one-dimensional geometry. These transitions give rise to several processes which are accessible to optical microscopy and spectroscopy: direct photon absorption, scattering of photons either elastically (Rayleigh scattering) or inelastically (Raman scattering), and luminescence from either optical or electrical excitation (fluorescence or electroluminescence, respectively). For SWNTs, the use of high end scientific cameras has allowed far-field microscopy to be performed, down to individual nanotubes. The earliest and most common approach is to build an image pixel by pixel by raster scanning a focused spot [1–4]. More recently, faster global imaging approaches have been used with fluorescence [5–8], Raman [9], and electroluminescence [10–12]. These approaches are like classical far-field optical microscopy, in which an entire image is obtained instantaneously. Classical microscopy also divides into bright field and dark field approaches, and thus far, bright field has been the main method for single nanotube imaging and spectroscopy.

In carbon nanotubes, optical dipoles have very strong polarization anisotropy ("antennae effects"), and both Raman and luminescence from SWNTs show a maximum response for light polarization along the nanotube axis [13, 14]. In dark field methods, improved contrast is obtained by preventing unwanted light from reaching the viewer/detector. Given this optical

Address correspondence to Jacques Lefebvre, jacques.lefebvre@nrc.ca; Paul Finnie, Paul.Finnie@nrc.ca

anisotropy or birefringence, a dark field method based on polarized light should be well suited to image carbon nanotubes.

Birefringence is widely used to characterize materials in various fields from metallurgy to biology. The technique is called polarized light microscopy (PLM) and specialized microscopes are made for this purpose [15]. In PLM, a pair of polarizers (with or without retarder waveplates) is rotated to orthogonality, blocking any transmitted light in absence of image specimen (or reflected light, if PLM is being performed in reflection). Insertion of a specimen between the polarizer pair assembly will reveal the birefringent (but otherwise potentially transparent) object as bright over the dark background. Although PLM has been extensively used to characterize synthetic and natural fibres with geometrical similarity to carbon nanotubes [16, 17], we have not found any PLM work on nanometre diameter fibres. PLM has been used to characterize films consisting of vast numbers of carbon nanotubes embedded in a matrix where the technique is useful as a means of assessing the degree of nanotube alignment [18–21].

In this paper, we report on polarized light microscopy imaging and spectroscopy of a single-walled carbon nanotube suspended in air over a slit. In contrast with other single nanotube optical imaging methods such as fluorescence imaging or global Raman imaging [5–7], PLM does not rely on high performance cameras. While the fluorescence intensity from a single nanotube can be strong, nearly all nanotube species emit in the near- to mid-infrared and typically only high end scientific cameras can achieve the right level of sensitivity in this spectral range. Global Raman imaging, on other the hand, can be performed in the visible range where cameras are most sensitive, but the Raman scattering cross-section from a single nanotube is generally so weak that a high performance camera is required. For PLM, the signal is strong and images can be obtained with a basic, uncooled CCD camera. Moreover, the technique applies to every nanotube type, whether single-, double- or multi-walled, metallic or semiconducting, be they bundled or individualized. To perform hyperspectral imaging, we have combined PLM with a tunable laser source to obtain the excitation profile. We found an exact match with fluorescence excitation spectroscopy performed simultaneously.

2. Results and discussion

Samples used in this work consisted of carbon nanotubes grown by chemical vapor deposition in a cold wall chamber. For growth around 850 °C at atmospheric pressure using dilute acetylene source gas, Co catalyst and a water vapor and hydrogen co-flow, samples were produced containing a significant number of ultralong SWNTs. Growing them on lithographically patterned gratings of ~20 μm pitch on silicon dioxide resulted in long (>10 μm) suspended lengths which emitted bright fluorescence (PL). Figure 1(a) is a low magnification PL image taken with an InGaAs camera (detection between 1000 and 1650 nm) and a 405 nm laser defocused to illuminate a large area. The image reveals a large number of nanotubes running roughly parallel to one another, a consequence of directional gas flow during synthesis [22–24]. We found that for our samples, many long suspended nanotubes are only loosely attached to the substrates and readily transfer upon contact with other surfaces, and they can remain suspended if transferred to a textured surface. For this work, we have transferred ultralong SWNTs to copper disk foils with multiple slits. Although the yield for this process is fairly low, more sophisticated approaches have been demonstrated for reliable transfer of suspended nanotubes [25]. Figure 1(b) is a luminescence image showing a transferred SWNT suspended across a 43 μm wide slit opening. Working with a freely suspended nanotube over an aperture is not essential for PLM but it is the best possible case since there is no background scattering.

Figure 1(c) provides an illustration of the experimental setup. The home-built polarized light microscope consists of four principal elements, two Glan–Thomson polarizers (extinction ratio greater than 10^6:1) and two polarization preserving microscope objectives (20 ×, 0.4 NA for illumination and 50 ×, 0.55 NA for imaging). The overall extinction ratio of the system is 500 000:1 as determined by measuring the power at co- and cross-polarized configurations and taking the ratio. The illumination stage consists of a tunable Ti-sapphire laser, a rotating holographic diffuser (0.5° diffusion angle) and a spatial filter (20 μm

pinhole and 20× collimating objective). The tunable laser (700–1000 nm) is used to enable hyperspectral imaging and *(n,m)* chirality assignment. The excitation power was approximately 15 kW/cm^2. The diffuser is necessary to reduce speckles which originate from the use of a coherent light source. The spatial filter is used to shape the illumination area to ensure that a minimal amount of light scatters off of the slit edges. Not shown in Fig. 1(c) is a sample stage with in-plane rotation to ensure proper alignment of the nanotube with respect to the polarizer pair. PLM images are acquired with a Lumenera Infinity2 color CCD camera (infrared blocking filter removed) with integration times between 100 ms and 400 ms. In addition to this,

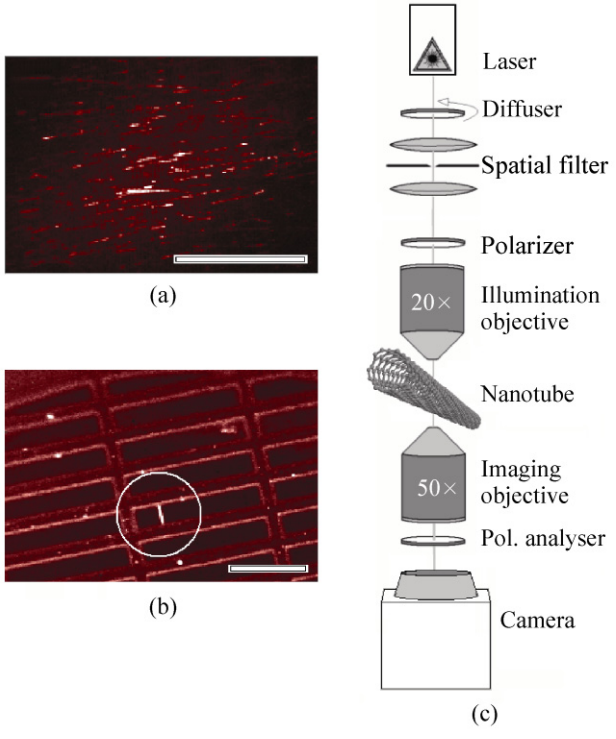

Figure 1 Carbon nanotube sample and experimental details. (a) PL image of aligned air suspended single walled carbon nanotubes (SWNTs) supported by grating textured substrate. The scale bar is 500 μm. (b) PL image of a suspended SWNT on a copper grid following transfer from contact to an air suspended nanotube sample. The scale bar is 200 μm. (c) Experimental setup. The polarized light microscope consists of two Glan–Thomson polarizers (Polarizer and Pol. Analyser) and two microscope objectives, one for illumination and one for imaging. The camera is mounted with a 250 mm imaging lens (not shown). Uniform illumination of the sample is obtained from a tunable Ti-sapphire laser which passes through a holographic diffuser and a spatial filter

the PLM leg, a PL imaging leg with a cooled InGaAs camera is used to simultaneously acquire the nanotube infrared emission (See, e.g., Ref. [6] for a typical PL setup). This combination of complementary methods is not essential but it serves to validate PLM for nanotube studies.

To estimate how sensitive a PLM microscope would have to be to image a single carbon nanotube, consider two parameters: the geometrical dimension of the nanotube and its absorption cross-section. Assuming that the microscope has 1 μm spatial resolution, a 1 nm nanotube will only cover a minute portion of the resolved length. For a long nanotube, longer than the spatial resolution, 1/1000 photons in any resolved spot can be considered to impinge on the nanotube. Of the photons impinging this reduced geometrical area, only a fraction will be absorbed by the nanotube. Using numbers from the literature, the optical cross section for a 1 micron segment of 1 nm diameter nanotube is 10^{-4}–10^{-5} μm^2 ($\sigma = 10^{-17}$–10^{-18} cm^2/carbon for the absorption cross section [26, 27]. We used the surface density of 0.054 nm^2/carbon of graphene.). Any absorbed or scattered photon will contribute to the PLM signal. The PLM signal should be comparable to the background signal to give a visibility of unity. In the worst case of 10^{-5} μm^2 optical cross section the required cross polarized rejection for a PLM system should be 100 000:1. With the 500 000:1 rejection of the microscope here, we anticipate from absorption alone, a signal to background visibility of 5:1. However, as will be discussed below, the image contrast cannot be explained on the basis of absorption alone but arises from the mixing of incident and nanotube related fields.

Two PLM images are shown in Figs. 2(a) and 2(b). Polarizer and analyser (see Fig. 1(c)) were set at 90° to minimize the direct transmitted light from the laser. Unblocked background light is seen as a white disk approximately 20 μm in diameter. This corresponds to the image of the pinhole aperture from the spatial filter. Non-uniformities in the illumination and light scattering from slit edges cause some streakiness in the background. The slit edges appear very bright as they efficiently scramble the polarization. In PLM images, SWNTs show up either as dark or bright over the 20 μm diameter background disk. We can confidently assign

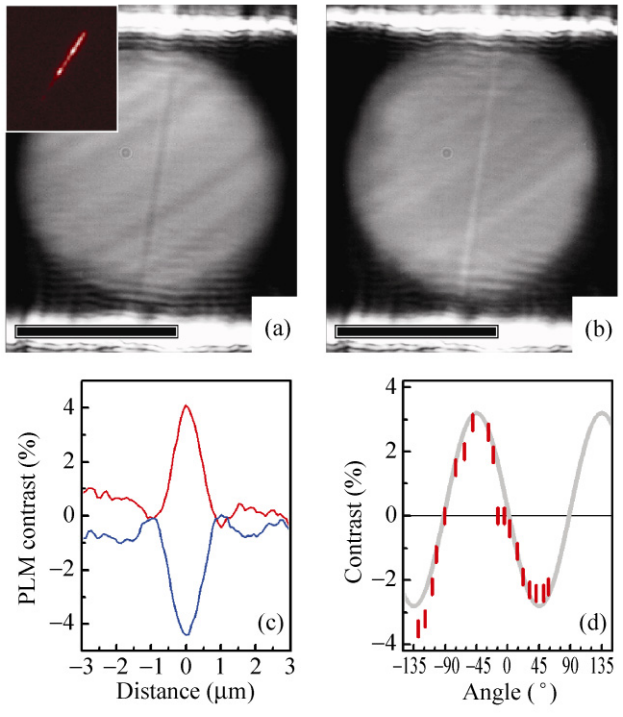

Figure 2 Polarized light microscopy of a carbon nanotube. (a, b) PLM image of a luminescent single walled carbon nanotube suspended across a 43 μm slit. The contrast is dark or bright depending on the polarizer and analyser angle with respect to the nanotube. The inset shows a luminescence image acquired simultaneously (the nanotube angle is slightly different from PLM). (c) Measured contrast obtained from (a) in blue and (b) in red. (d) Rotation dependence of PLM contrast of a single walled carbon nanotube. The angle is measured between the nanotube and the analyser (see supplementary information). The continuous line is a sin2β functional form

the nanotube to the single walled type, since PL was simultaneously performed and used to locate the SWNT on the copper grid. In addition, PL excitation reveals a single dominant resonance, which can be identified as an E_{22} resonance.

Nanotubes are ideal to image by PLM because they have strong optical anisotropy [13, 14, 28]. They therefore act like a third polarizer in the system and allow for some light to leak through the polarizer–analyser pair. We therefore expected a nanotube to appear bright over dark background. This is indeed what Fig. 2(b) shows. We found however that depending on the exact polarizer–analyser–nanotube alignment, a dark contrast over a dark background is also equally possible.

Figure 2(c) shows the measured contrast obtained from averaging line intensities perpendicular to the nanotube for both Figs. 2(a) and 2(b) (the contrast is given by the ratio of the number of counts from the nanotube to that of the background). It shows one main peak and two side lobes of weak intensity. From the main peak, we extract an imaging resolution of 1 μm. This value is likely limited by the length of the Glan–Thomson analyser (15 mm). The magnitude of the contrast is about 4% whether it is positive or negative (bright or dark, respectively). With the current setup, contrasts down to 0.4% could be detected but a tenfold improvement should be possible with better uniformity of illumination.

Compared to our initial estimate of 5:1, the contrast seen here is much smaller, by a factor of 100. It is known from light-induced birefringence in a gas that polarization spectroscopy has its maximum sensitivity when the polarizer/analyser angle is shifted slightly away from 90° [29, 30]. The dominant contribution to the signal consists of the product of incident and scattered fields rather than the scattered intensity alone. Measuring the effect of this mixing of fields is also known as homodyne detection. From calculations reported in the Electronic Supplementary Material (ESM) (Parts 1 and 2), we conclude that our first guess estimation of 100 000:1 is only valid for direct transmission of light. For a cross polarized configuration at exactly 90°, a thousandfold improvement in rejection would be required to see a carbon nanotube in absorption alone.

Rotation of the polarizer/analyser angle away from 90° might appear detrimental to the image contrast as more background light reaches the detector. However, the field leaking through the analyser is beneficial as it combines with the scattered field from the nanotube and leads to a measurable intensity on the camera (detectors are sensitive to the sum of fields squared rather than the sum of independently squared fields). The magnitude of this homodyne contribution greatly overwhelms the weak signal coming purely from nanotube absorption (numbers are given in the ESM, Part 2). We estimate that for perfect polarisers, a rotation as small as 0.2° is consistent with the level of contrast reported here. Alternatively, a rejection of 500 000:1 would give a 9% contrast.

We have looked more closely at how the contrast evolves for a fixed polarizer–analyser angle close to 90° while the nanotube is rotated (detailed results are available in the ESM, Part 3). Figure 2(d) shows a maximum contrast when the nanotube is at 45° and zero when the nanotube is parallel to either the polarizer or the analyser. Although this result is in agreement with initial expectations, we find that two quadrants have positive contrast and two have negative contrast. The calculation presented in the ESM (Part 4) shows that this reversal is fully consistent with homodyne signal being the dominant contribution. As shown in Fig. 2(d), the calculated $\sin 2\beta$ functional form fits the experimental data well.

Figure 3 compares a PLM image to a PL image taken from the same nanotube. For PLM in Fig. 3(b), the contrast appears quite uniform over the entire length of the nanotube. This is also evident in Fig. 3(c), where the intensity is plotted along the nanotube length. Although the scatter is quite substantial, we can say definitively that intensity changes are no greater than 25%, and there are no specific regions of high or low contrast. This is in striking contrast with the PL image in Fig. 3(a), where three regions of brighter emission are seen. Figure 3(c) shows that these bright areas correspond to an increase of as much as 80% compared to dimmer areas. This clearly demonstrates the relative sensitivity of PL to factors such as defects, and damage compared to absorption or scattering which cause the PLM signal. Luminescence will be reduced in intensity or even quenched if there are non-radiative decay channels. Since the exciton is mobile over scales of >100 nm [6–8], even dilute defect densities can significantly reduce the PL efficiency. In contrast, the effect of defects on absorption and scattering is much less significant.

Semiconductor SWNTs have strong absorption and scattering resonances related to E_{11} and E_{22} dipole allowed transitions. Using a tunable light source makes PLM a hyperspectral imaging method, and we can use this to identify the resonances. Figure 4 shows how the PLM contrast from a SWNT is sensitive to the laser wavelength. At 1.7 eV (730 nm), the contrast is a maximum at 4% and a threefold reduction is measured when moving away from the resonance. We have performed PL excitation (PLE) measurements

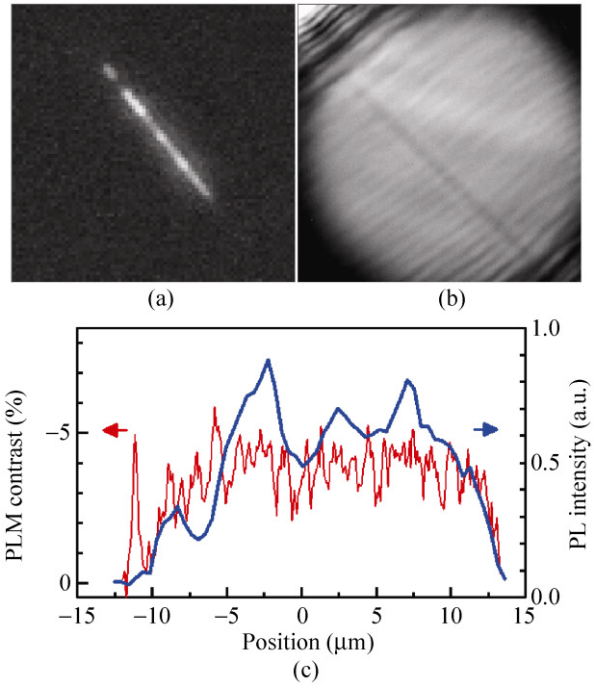

Figure 3 Spatial fluctuations of fluorescence and PLM intensity. (a, b) Fluorescence (PL) and PLM images of a single-walled carbon nanotube for resonant excitation at 730 nm (1.70 eV). Scales in (a) and (b) have been approximately matched. (c) PL (blue) and PLM (red) intensity versus position along the nanotube length. The scales for PL and PLM have been approximately matched and the positions are not precisely the same. Compared to image (a) and (b), the position scale runs from upper left to lower right

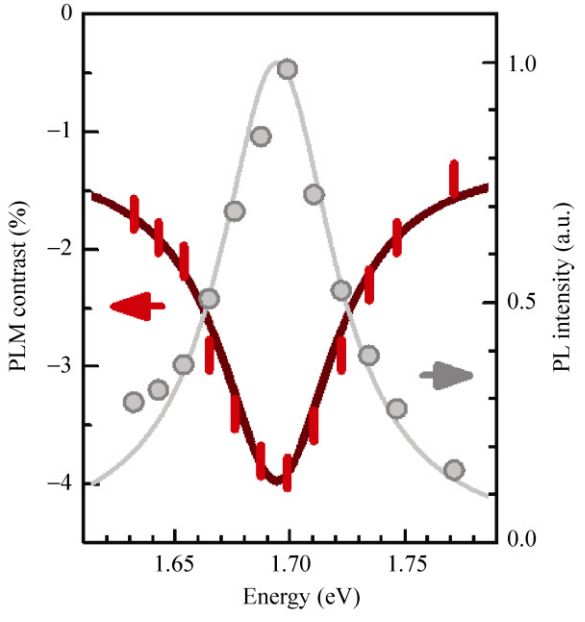

Figure 4 Resonance profile. Fluorescence (gray) and PLM (color) intensity versus laser energy reveals a matching resonance at E_{22} (corresponding images at resonance are shown in Figs. 3(a) and 3(b)). Continuous lines are a Lorentzian fit with E_0 = 1.694 eV and FWHM = 30 meV. This nanotube is assigned to the (10,2) species

simultaneously and assigned the resonance to E_{22}. Both resonances (in PL and PLM) can be fitted with a Lorentzian functional form with a common E_{22} energy and linewidth (1.694 eV and 30 meV, respectively). This demonstrates that PLM provides similar information to PLE and could likewise be used as a characterization method.

3. Conclusions

In this work, we have demonstrated that polarized light microscopy can be used to image individual single-walled carbon nanotubes. The polarized light microscope has a simple design and does not require a high end camera or light source. Although the work focused on luminescent semiconductor SWNTs, the technique should also be suitable to image other nanotube types (whether metallic, multi-walled or bundled) and nanowires. Although experimentally more challenging, PLM based on circularly polarized light could potentially differentiate between nanotube handedness. Beyond simple imaging, PLM can be extended to provide hyperspectral capability, enabling the assignment of optical transitions, and nanotube chiralities. Since PLM is not limited by the sensitivity of available detectors, the spectral signature of large diameter nanotubes and the like should be observable. It appears that PLM should become an integral part of the optical toolset for the study of carbon nanotubes and related materials.

Acknowledgements

Our special thanks go to P. Marshall, H. Tran, P. Waldron, and P. Chow-Chong for their technical support and expertise in sample fabrication and nanotube synthesis. We are grateful to an anonymous reviewer for their insight with respect to homodyne detection.

Electronic Supplementary Material: One additional figure showing PLM images of a SWNT for several rotation angles and three calculations of the contrast relevant to experimental conditions are available in the online version of this article at http://dx.doi.org/10.1007/s12274-011-0135-8.

References

[1] Mews, A.; Koberling, F.; Basché, T.; Philipp, G.; Duesberg, G. S.; Roth, S.; Burghard, M. Raman imaging of single carbon nanotubes. *Adv. Mater.* **2000**, *12*, 1210–1214.

[2] Sfeir, M. Y.; Wang, F.; Huang, L.; Chuang, C. -C.; Hone, J.; O'Brien, S. P.; Heinz, T. F.; Brus, L. E. Probing electronic transitions in individual carbon nanotubes by Rayleigh scattering. *Science* **2004**, *306*, 1540–1543.

[3] Kiowski, O.; Jester, S. -S.; Lebedkin, S.; Jin, Z.; Li, Y.; Kappes, M. M. Photoluminescence spectral imaging of ultralong single-walled carbon nanotubes: Micromanipulation-induced strain, rupture, and determination of handedness. *Phys. Rev. B* **2009**, *80*, 075426.

[4] Joh, D. Y.; Herman, L. H.; Ju, S. -Y.; Kinder, J.; Segal, M. A.; Johnson, J. N.; Chan, G. K. L.; Park J. On-chip Rayleigh imaging and spectroscopy of carbon nanotubes. *Nano Lett.* **2011**, *11*, 1–7.

[5] Tsyboulski, D. A.; Bachilo, S. M.; Weisman, R. B. Versatile visualization of individual single-walled carbon nanotubes with near-infrared fluorescence microscopy. *Nano Lett.* **2005**, *5*, 975–979.

[6] Lefebvre, J.; Austing, D. G.; Bond, J.; Finnie, P. Photoluminescence imaging of suspended single-walled carbon nanotubes. *Nano Lett.* **2006**, *6*, 1603–1608.

[7] Cognet, L.; Tsyboulski, D. A.; Rocha, J. -D. R.; Doyle, C. D.; Tour J. M.; Weisman, R. B. Stepwise quenching of exciton fluorescence in carbon nanotubes by single-molecule reactions. *Science* **2007**, *316*, 1465–1468.

[8] Yoshikawa, K.; Matsuda, K.; Kanemitsu, Y. Exciton transport in suspended single carbon nanotubes studied by photoluminescence imaging spectroscopy. *J. Phys. Chem. C* **2010**, *114*, 4353–4356.

[9] Kaminska, K.; Lefebvre, J.; Austing, D. G.; Finnie, P. Real-time global Raman imaging and optical manipulation of suspended carbon nanotubes. *Phys. Rev. B* **2006**, *73*, 235410.

[10] Freitag, M.; Chen, J.; Tersoff, J.; Tsang, J. C.; Fu, Q.; Liu, J.; Avouris, P. Mobile ambipolar domain in carbon-nanotube infrared emitters. *Phys. Rev. Lett.* **2004**, *93*, 076803.

[11] Lefebvre, J.; Austing, D. G.; Finnie, P. Two modes of electroluminescence from single-walled carbon nanotubes. *Phys. Stat. Solidi RRL* **2009**, *3*, 199–201.

[12] Zaumseil, J.; Ho, X.; Guest, J. R.; Wiederrecht, G. P.; Rogers, J. A. Electroluminescence from electrolyte-gated carbon nanotube field-effect transistors. *ACS Nano* **2009**, *3*, 2225–2234.

[13] Duesberg, G. S.; Loa, I.; Burghard, M.; Syassen, K.; Roth, S. Polarized Raman spectroscopy on isolated single-wall carbon nanotubes. *Phys. Rev. Lett.* **2000**, *85*, 5436–5439.

[14] Lefebvre, J.; Finnie, P.; Homma, Y. Photoluminescence from an individual single-walled carbon nanotube. *Phys. Rev. B* **2004**, *69*, 075403.

[15] Davidson, M. W.; Lofgren, G. E. Photomicrography in the geological sciences. *J. Geol. Educ*. **1991**, *39*, 403–418.

[16] Stoeffler, S. E. A flowchart system for the identification of common synthetic fibers by polarized light microscopy. *J. Forensic Sci.* **1996**, *41*, 297–299.

[17] McCrone, W. C. Identification of asbestos by polarized light microscopy. In *Proc. Workshop on Asbestos: Definitions and Meas. Methods*, **1978**, 235–248.

[18] Ramesh, S.; Ericson, L. M.; Davis, V. A.; Saini, R. K.; Kittrell, C.; Pasquali, M.; Billups, W. E.; Adams, W. W.; Hauge, R. H.; Smalley, R. E. Dissolution of pristine single walled carbon nanotubes in superacids by direct protonation. *J. Phys. Chem. B* **2004**, *108*, 8794–8798.

[19] Yin, C. -L.; Liu, Z. -Y.; Yang, W.; Yang, M. -B.; Feng, J. -M. Crystallization and morphology of iPP/MWCNT prepared by compounding iPP melt with MWCNT aqueous suspension. *Colloid Polym. Sci.* **2009**, *287*, 615–620.

[20] Zhang, J. -C.; Luo, R. -Y.; Wu, X. -W.; Li, Q. Fabrication and characteristics of carbon nanofiber-reinforced carbon/carbon composites by fast catalytic infiltration processes. *Chem. Vap. Deposition* **2009**, *15*, 33–38.

[21] Parra-Vasquez, A. N. G.; Behabtu, N.; Green, M. J.; Pint, C. L.; Young, C. C.; Schmidt, J.; Kesselman, E.; Goyal, A.; Ajayan, P. M.; Cohen, Y.; Talmon, Y.; Hauge, R. H.; Pasquali, M. Spontaneous dissolution of ultralong single- and multiwalled carbon nanotubes. *ACS Nano* **2010**, *4*, 3969–3978.

[22] Huang, S. M.; Cai, X. Y.; Liu, J. Growth of millimeter-long and horizontally aligned single-walled carbon nanotubes on flat substrates. *J. Am. Chem. Soc.* **2003**, *125*, 5636–5637.

[23] Zheng, L. X.; O'Connell, M. J.; Doorn, S. K.; Liao, X. Z.; Zhao, Y. H.; Akhadov, E. A.; Hoffbauer, M. A.; Roop, B. J.; Jia, Q. X.; Dye, R. C.; Peterson, D. E.; Huang, S. M.; Liu, J.; Zhu, Y. T. Ultralong single-wall carbon nanotubes. *Nat. Mater.* **2004**, *3*, 673–676.

[24] Jin, Z.; Chu, H. B.; Wang, J. Y.; Hong, J. X.; Tan, W. C.; Li, Y. Ultralow feeding gas flow guiding growth of large-scale horizontally aligned single-walled carbon nanotube arrays. *Nano Lett.* **2007**, *7*, 2073–2079.

[25] Huang, X. M. H.; Caldwell, R.; Huang, L.; Jun, S. C.; Huang, M.; Sfeir, M. Y.; O'Brien, S. P.; Hone, J. Controlled placement of individual carbon nanotubes. *Nano Lett.* **2005**, *5*, 1515–1518.

[26] Islam, M. F.; Milkie, D. E.; Kane, C. L.; Yodh, A. G.; Kikkawa, J. M. Direct measurement of the polarized optical absorption cross section of single-wall carbon nanotubes. *Phys. Rev. Lett*. **2004**, *93*, 037404.

[27] Berciaud, S.; Cognet, L.; Lounis, B. Luminescence decay and the absorption cross section of individual single-walled carbon nanotubes. *Phys. Rev. Lett.* **2008**, *101*, 077402.

[28] Lefebvre, J.; Finnie, P. Polarized photoluminescence excitation spectroscopy of single-walled carbon nanotubes. *Phys. Rev. Lett.* **2007**, *98*, 167406.

[29] Wieman, C.; Hänsch, T. W. Doppler-free laser polarization spectroscopy. *Phys. Rev. Lett.* **1976**, *36*, 1170–1173.

[30] Demtröder, W. *Laser Spectroscopy: Basic Concepts and Instrumentation*, 3rd ed; Springer: Berlin, New York, 2003.